



## Charge transport mechanisms and magnetoresistance behavior of $\text{La}_{0.6}\text{Pr}_{0.1}\text{Ca}_{0.3}\text{MnO}_3$ manganite



Sapana Solanki<sup>a</sup>, Davit Dhruv<sup>a,e</sup>, Hetal Boricha<sup>a</sup>, Alpa Zankat<sup>a</sup>, K.N. Rathod<sup>a</sup>, Bhargav Rajyaguru<sup>a</sup>, R.K. Trivedi<sup>b</sup>, A.D. Joshi<sup>c</sup>, S. Mukherjee<sup>d</sup>, P.S. Solanki<sup>a</sup>, N.A. Shah<sup>a,\*</sup>

<sup>a</sup> Department of Physics, Saurashtra University, Rajkot, 360 005, India

<sup>b</sup> H. & H.B. Kotak Science College, Saurashtra University, Rajkot, 360 005, India

<sup>c</sup> Department of Nanoscience and Advanced Materials, Saurashtra University, Rajkot, 360 005, India

<sup>d</sup> UGC-DAE Consortium for Scientific Research, Mumbai Centre, B.A.R.C. Campus, Mumbai, 400 085, India

<sup>e</sup> Department of Physics, Marwadi University, Rajkot, 360 003, India

### ARTICLE INFO

#### Keywords:

Solid state reaction  
Manganite  
Magnetotransport  
Magnetoresistance

### ABSTRACT

Structural properties and charge conduction mechanisms in  $\text{La}_{0.6}\text{Pr}_{0.1}\text{Ca}_{0.3}\text{MnO}_3$  (LPCMO) manganite has been studied. Presently studied LPCMO manganite was successfully synthesized by solid state reaction method. Structural studies using X-ray diffraction (XRD) measurement at room temperature confirm single phase orthorhombic unit cell without any impurity. A methodical investigation of electrical resistivity was undertaken, for both, as a function of temperature as well as magnetic field. It is observed that LPCMO sample shows metal to insulator transition at  $T_p$  as well as low resistivity upturn around 30K. Various models and mechanisms have been studied to verify the charge transport properties for low temperature upturn, metallic behavior as well as insulating/semiconducting behavior. Magnetoresistance (MR) behaviors at different temperatures have been theoretically understood on the basis of contributions from grain and grain boundaries.

### 1. Introduction

During last decade, mixed valent manganites with general formula  $R_{1-x}A_x\text{MnO}_3$  (where, R is the trivalent rare-earth ion and A is a divalent alkaline earth ions i.e. Ba, Sr, Ca, etc) were widely studied for their interesting and extraordinary physical properties. Large number of studies on the colossal magnetoresistance (CMR) has been executed in the case of single crystals [1], thin films [2] and ceramic CMR materials [3]. In such manganite systems, the mechanisms for conduction and different magnetic phase transitions are relevant to the amount of doping and temperature. The parent compound  $\text{LaMnO}_3$  (undoped) behaves as an insulator with antiferromagnetically coupled trivalent manganese ions through super-exchange mechanism. The electronic configuration of  $\text{Mn}^{3+}$  is  $t^3 2g^1$ . In manganites, holes can be introduced with partial substitution of trivalent rare earth ions with divalent alkaline earth metals. As a result,  $e_g$  electron has tendency to hop between  $\text{Mn}^{3+}$  and  $\text{Mn}^{4+}$  ions through oxygen ions, according to zener double exchange (ZDE) mechanism. This double exchange (DE) mechanism gives rise to metallic nature associated with ferromagnetism in these compounds. However, DE mechanism alone cannot explain all the aspects of CMR

effect. The prime details of resistivity-temperature curves can be understood by Jahn-Teller distortion of  $\text{Mn}^{3+}$  ions [4], charge ordering [5], size of rare-earth ions and doped alkaline earth ions (i.e. size disorder) [6], spin ordering [7], tolerance factor [8], electron-phonon coupling [9], electron-electron scattering [9], phase separation [7], etc. In manganites, all these aspects can be controlled by various external parameters such as synthesis method used [10], temperature [11], pressure [12], applied magnetic field [13], applied electric field [14], sintering temperature [15], annealing temperature [16], etc.

It is well known that,  $\text{La}_{0.7}\text{Ca}_{0.3}\text{MnO}_3$  exhibits phase transition at temperature  $\sim 260\text{K}$ . This compound has been studied widely in every form including polycrystalline bulk [17], nanostructure [18], thin film [19], composite [17,18], etc. In this system, partial substitution of lanthanum by other rare-earth/s (Dy, Nd, Tb, Eu, etc) generates interesting physical phenomena [20,21]. This type of substitution does not affect amounts of  $\text{Mn}^{3+}$  and  $\text{Mn}^{4+}$  ions but enhances structural and magnetic disorders in the lattice because of the decrease in average ionic radius. Altintas et al. [22] have studied structural and magneto-electrical properties of  $\text{La}_{0.7-x}\text{Eu}_x\text{Ca}_{0.3}\text{MnO}_3$  ( $x = 0.0$  and  $0.1$ ). Sen et al. [23] have studied structural, magnetotransport and morphological studies of Sb

\* Corresponding author.

E-mail address: [snikesh@yahoo.com](mailto:snikesh@yahoo.com) (N.A. Shah).

doped  $\text{La}_{2/3}\text{Ba}_{1/3}\text{MnO}_3$ . Zainullinaa et al. [24] have studied elastic and magnetic properties of  $\text{La}_{0.6}\text{Pr}_{0.1}\text{Ca}_{0.3}\text{MnO}_3$  single crystal. Rozenberg et al. [25] studied the effect of Ag content on the low temperature resistivity minimum behavior of mixed valent  $\text{La}_{0.5}\text{Pb}_{0.5}\text{MnO}_3$  manganites. Solanki et al. [26] have analyzed transport studies on  $\text{La}_{0.8-x}\text{Pr}_{0.2}\text{Sr}_x\text{MnO}_3$  manganites.

In this communication, different models and mechanisms have been taken into consideration to understand the low temperature resistivity minimum behavior, metallic behavior, insulating/semiconducting nature and magnetoresistive behavior for structural, transport and magnetotransport studies on LPCMO manganite compound. It is important to note that  $\text{Pr}^{3+}$  has been selected for a partial substitution mainly due to (i) the cationic size of  $\text{Pr}^{3+}$  ion is smaller than lanthanum ion ( $\text{La}^{3+}$ ) which results in the reduction in Mn–O–Mn bond angle from  $180^\circ$  as a result, super-exchange becomes competitive with ZDE mechanism [27, 28], (ii)  $\text{Pr}^{3+}$  has the value of magnetic moment  $\sim 3.4\mu_B$  as compared to  $\text{La}^{3+}$  (i.e. zero magnetic moment) which strongly affects the MR properties of presently studied LPCMO manganite [27–31]. It is noteworthy that use of Pr as a dopant at La site in La based manganite compounds can make following anomaly: generally, solid state reaction process requires  $\text{Pr}_6\text{O}_{11}$  as a starting material that provides mixed ionic valent states of Pr, i.e. 3+ and 4+, in the manganite lattice. This may create a strong impression or affection on the transport, magnetic and magnetoresistive properties of particular manganite [29]. To overcome this issue of ionic mixed valent states of Pr and to have better control over the Pr oxidation state, one can use sol–gel method (instead of solid state reaction route) to prepare Pr based manganite compounds, since Pr acetate or Pr nitrate or Pr oxalate or other Pr based starting materials are being used as precursor in the process that deal with single valance state of Pr (i.e. 3+) [32]. Although, it is also well known fact that nanostructured manganites possess defective structure having large number of oxygen vacancies (as compared to its micron sized polycrystalline or bulk phase) [15]. This possibility of creation of oxygen vacancies in any sol–gel grown manganite lattice alters its transport and other properties effectively through the change in Mn valance states. Similar aspects of Pr valance states have also been considered for Pr based 123 superconductors (i.e.  $\text{Pr}_1\text{Ba}_2\text{Cu}_3\text{O}_7$ ) wherein sol–gel method has been used [33,34]. Also, one can employ Nd as a dopant instead of Pr at La site to study the doping effect of Nd on transport, magnetic and magnetoresistive properties of particular manganites [20]. The use of Nd as a dopant at La site in manganite, instead of Pr, can create comparatively large ionic size mismatch due to larger difference between the  $\text{Nd}^{3+}$  (1.163 Å) and  $\text{La}^{3+}$  (1.216 Å) as compared to the ionic size mismatch between the  $\text{Pr}^{3+}$  (1.179 Å) and  $\text{La}^{3+}$  (1.216 Å) ions. In fact, our aim of the present work is to consider LPCMO manganite lattice for understanding the effect of magnetic field on its charge transport properties. In this study, we have expected structurally (so-called) perfect lattice of manganite therefore we have employed solid state reaction method to prepare the sample that, again, may create the issue of mixed valent states of Pr in its lattice. However, our complete study deals with the effect of magnetic field on the charge transport properties and mechanisms of LPCMO manganite compound wherein only single composition (with the Pr content of 10% at La site) is involved. Hence, whatever the mixed valent states of Pr exists in the lattice that remains same throughout the study. Even though, prior to proceed further for understanding and explanation of the obtained results, it is necessary here to highlight the estimated value of oxygen content through iodometric titration method for presently targeted LPCMO stoichiometry  $\sim 2.98$  which reflects and confirms better stoichiometry of the compound under study.

## 2. Experimental technique

Polycrystalline bulk sample of  $\text{La}_{0.6}\text{Pr}_{0.1}\text{Ca}_{0.3}\text{MnO}_3$  was synthesized using standard solid state reaction route. High purity lanthanum oxide ( $\text{La}_2\text{O}_3$ ), praseodymium oxide ( $\text{P}_6\text{O}_{11}$ ), calcium carbonate ( $\text{CaCO}_3$ ) and manganese oxide ( $\text{MnO}_2$ ) were selected as starting materials in

appropriate stoichiometric ratio and heated in the furnace for making them dry. The materials were ground for 3 h for preparing homogeneous mixture. This mixture was heated for first calcination at  $900^\circ\text{C}$  for 24 h followed by again ground for 3 h. The second calcination was done at  $1100^\circ\text{C}$  for 24 h. After all the calcinations, material was re-grounded and pelletized in 10 mm disc shape form. Final heating for sintering purpose was carried out at  $1250^\circ\text{C}$  for 72 h. Fig. 1 depicts the steps involved in the solid state reaction route presently employed to prepare LPCMO manganite compound. Structural study was carried out using XRD measurement recorded on Philips diffractometer (PW 3040/60, X'pert PRO) using  $\text{Cu K}\alpha$  radiation at room temperature (RT). To study the resistivity under different applied magnetic fields and MR behaviors at different temperatures, transport measurements were carried out using four probe method in the temperature range of 5–325 K in the field range of 0 to 10 T using physical property measurement system (14T DynaCool PPMS; Quantum Design).

## 3. Results and discussion

XRD pattern of the LPCMO sample under study was recorded at room temperature for the  $2\theta$  range of  $10^\circ$  to  $120^\circ$ . One can confirm the quality of the structure of the compound by performing Rietveld refinements of the pattern, presented in Fig. 2. Rietveld refinements suggest the single phase nature of the sample with distorted orthorhombic cell structure. It possesses  $Pnma$  space group (no. 62) [35] with the lattice parameters and cell volume, as shown in Table 1. Structure of  $\text{La}_{0.6}\text{Pr}_{0.1}\text{Ca}_{0.3}\text{MnO}_3$  manganite has already been previously reported in its single crystal form and reported space group is  $Pnma$  (no. 62) [24,36–38]. Table 1 also lists the values of Mn–O–Mn bond angle (average for epical and basal planes) and Mn–O bond length (average of epical and basal planes) as well as R-factors obtained from the Rietveld refinements. It also provides values of different crystallographic positions of all elements present in the studied stoichiometry of the sample and their thermal displacements. One can understand that there exists deviation in the Mn–O–Mn bond angle from its ideal value of  $\sim 180^\circ$  for presently studied LPCMO manganite. This can be ascribed to the presence of smaller ionic radius of  $\text{Pr}^{3+}$  at  $\text{La}^{3+}$  site in LPCMO manganite lattice. Cherif et al. [39] have studied the series of  $\text{La}_{0.6}\text{Pr}_{0.1}\text{Sr}_{0.3}\text{Mn}_{1-x}\text{Fe}_x\text{O}_3$  manganites wherein Fe-free manganite compound (i.e.  $\text{La}_{0.6}\text{Pr}_{0.1}\text{Sr}_{0.3}\text{MnO}_3$ ) possesses rhombohedral unit cell structure. This difference in unit cell structures of reported  $\text{La}_{0.6}\text{Pr}_{0.1}\text{Sr}_{0.3}\text{MnO}_3$  (rhombohedral) and presently studied LPCMO compound (distorted orthorhombic) is due to the difference in the ionic radius of  $\text{Sr}^{2+}$  and  $\text{Ca}^{2+}$  ions doped at  $\text{La}^{3+}$  site in their respective manganite lattices.

Resistivity measurements of LPCMO manganite have been performed as a function of temperature under different applied magnetic fields (0, 2, 4, 6, 8 and 10 T). The obtained experimental results are shown in Fig. 3. The following features can be observed from Fig. 3:

- LPCMO sample exhibits metal ( $d\rho/dt > 0$ ) to insulator ( $d\rho/dt < 0$ ) phase transition ( $T_p$ ) with increase in temperature (as indicated by upward arrow in Fig. 3).
- Resistivity gets suppressed with applied magnetic field indicating the presence of negative MR [ $\text{MR\%} = \{(\rho_0 - \rho_H)/\rho_0\} \times 100$ ] for the present case of LPCMO manganite.
- The transition temperature ( $T_p$ ) shifts towards higher temperature throughout the whole magnetic field range studied. This can be the attribution of applied magnetic field which delocalizes the charge carriers thereby reducing the resistivity. As a result, the metallic region might have suppressed the insulating region which consequences in an enhancement of  $T_p$  under application of magnetic field.

It is worth here to highlight some comparative aspects of resistivity behavior observed for the presently studied LPCMO compound (Fig. 3) and other reported rare earth (including yttrium) doped similar

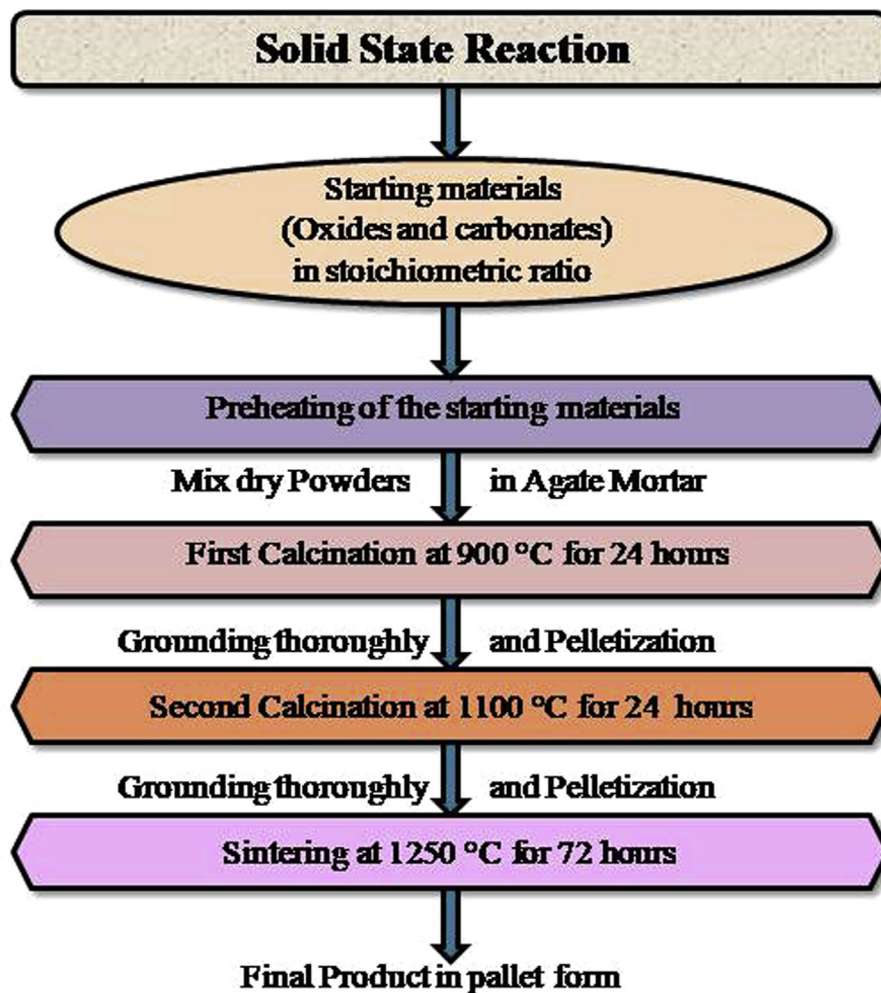


**Fig. 1.** Steps followed in the solid state reaction route used for the preparation of LPCMO sample.

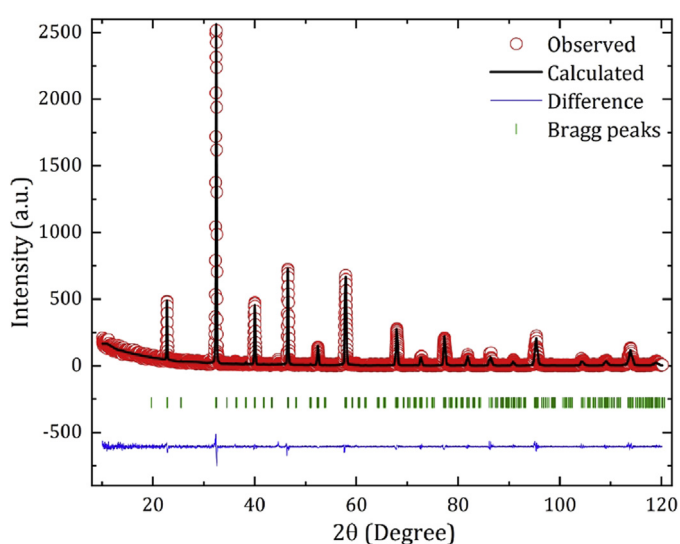


**Fig. 2.** Rietveld refined X-ray diffraction pattern of LPCMO sample.

compounds [i.e.  $\text{La}_{0.6}\text{R}_{0.1}\text{Ca}_{0.3}\text{MnO}_3$  (LRMCO); R = Y, Eu, Ho, Nd, Sm, Gd and Dy] [22,40–42]. Presently studied LPCMO compound shows  $T_p$  at  $\sim 222\text{K}$  (under zero magnetic field) which is much higher than the values of  $T_p$  for Eu (165K [22]), Y (171K [40]), Ho ( $\sim 100\text{K}$  [41]), Y ( $\sim 75\text{K}$

[41]), Nd (187K [42]), Sm (151K [42]), Gd (130K [42]) and Dy (114K [42]) based LRCMO compounds under zero magnetic field. This suggests that presently studied LPCMO compound is not only worth to study but also better suitable for targeted practical applications. For the comparison of peak resistivity (i.e. resistivity at  $T_p$ ), presently studied LPCMO compound exhibits lower zero magnetic field peak resistivity ( $\sim 1.217\Omega\text{cm}$ ) as compared to all other reported LRCMO compounds as Eu ( $\sim 22\Omega\text{cm}$  [22]), Y ( $\sim 10.5\Omega\text{cm}$  [40]), Ho ( $\sim 175\Omega\text{cm}$  [41]), Y ( $\sim 2300\Omega\text{cm}$  [41]), Gd ( $\sim 12.78\Omega\text{cm}$  [42]) and Dy ( $\sim 60\Omega\text{cm}$  [42]) based LRCMO compounds under zero magnetic field. Although, LRCMO compounds with Nd ( $\sim 0.28\Omega\text{cm}$  [42]) and Sm ( $\sim 2.52\Omega\text{cm}$  [42]) show lower resistivity values than present LPCMO sample which may be due to fact that Nd and Sm based LRCMO nanostructured manganites possess comparatively lower average Mn–O bond lengths (Nd:  $1.9603\text{\AA}$  and Sm:  $1.9577\text{\AA}$ ) than presently studied LPCMO manganite compound having an average Mn–O bond length (Pr:  $2.1781$ ; Table 1). As a result, LRCMO (R = Nd and Sm) compounds possess lower resistivity than LPCMO manganite. However, precise understanding of the explanation for resistivity value based comparison between Nd (reported [42]), Sm (reported [42]) and Pr (present study) samples require further in-depth investigations.

As shown in Fig. 3, LPCMO sample exhibits a resistivity upturn at low temperature (as indicated by downward arrow in Fig. 3) which means there exists decrease in resistivity from  $5\text{K}$  to  $T_{up}$ , then increase in resistivity from  $T_{up}$  to  $T_p$  (i.e. resistivity upturn transition) followed by decrease in resistivity from  $T_p$  to  $325\text{K}$  (i.e. insulator to metal transition).

**Table 1**  
Rietveld refined parameters for LPCMO manganite.

Sample	La <sub>0.6</sub> Pr <sub>0.1</sub> Ca <sub>0.3</sub> MnO <sub>3</sub>			
a (Å)	5.5101 (4)			
b (Å)	7.7958 (2)			
c (Å)	5.5328 (3)			
V (Å <sup>3</sup> )	237.66 (6)			
Structure type	Orthorhombic			
Space group	Pnma (no. 62)			
Mn–O–Mn bond angle (o)	160.96 (4) (average)			
Mn–O bond length (Å)	2.1782 (2) (average)			
RP (%)	11.5			
RWP (%)	13.4			
REXP (%)	7.33			
Goodness of fit ( $\chi^2$ )	1.42			
Atoms	Atomic Positions ( $\pm$ Deviations)		Thermal Displacements	
	X	Y	Z	
			B	
La	0.00108 ( $\pm$ 0.00085)	0.25000 ( $\pm$ 0.00000)	1.00184 ( $\pm$ 0.00117)	0.97227 ( $\pm$ 0.01796)
Pr	0.00108 ( $\pm$ 0.00085)	0.25000 ( $\pm$ 0.00000)	1.00184 ( $\pm$ 0.00117)	0.97227 ( $\pm$ 0.01796)
Ca	0.00108 ( $\pm$ 0.00085)	0.25000 ( $\pm$ 0.00000)	1.00184 ( $\pm$ 0.00117)	0.97227 ( $\pm$ 0.01796)
Mn	0.00000 ( $\pm$ 0.00000)	0.00000 ( $\pm$ 0.00000)	0.50000 ( $\pm$ 0.00000)	0.92368 ( $\pm$ 0.04943)
O1	0.40742 ( $\pm$ 0.00876)	0.25000 ( $\pm$ 0.00000)	0.02819 ( $\pm$ 0.01489)	2.26161 ( $\pm$ 0.19135)
O2	0.26796 ( $\pm$ 0.00504)	0.02174 ( $\pm$ 0.00159)	0.73801 ( $\pm$ 0.00455)	2.26396 ( $\pm$ 0.19135)

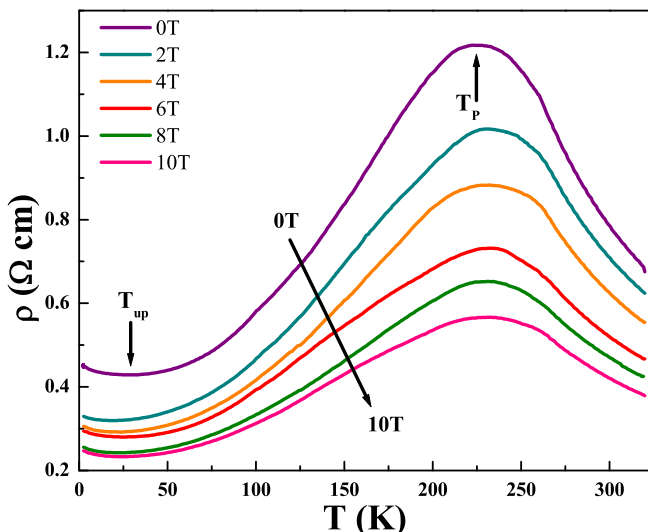


**Fig. 3.** Temperature dependent electrical resistivity plots under several magnetic applied fields for LPCMO sample.

In this regard, LPCMO sample is found to exhibit two electronic transitions in resistive curve: (1) predominantly, one can be observed at  $T_p$  which is known as insulator to metal (I–M) transition and (2) metal to insulator (M–I) transition at low temperature ( $T < 50\text{K}$ ), known as  $T_{\text{up}}$  below which the resistivity increases with decrease in temperature. In LPCMO sample, the resistivity upturn  $T_{\text{up}}$  is also found to get suppressed with increasing magnetic field. The origin of resistivity upturn might be considered from spin dependent scattering which is reduced under the applied magnetic field.

Resistivity can be considered as resultant effect of a competition between the elastic scattering (electron–impurity interaction and coulomb interaction between the charge carriers) and inelastic scattering (electron–phonon interaction) ( $\rho = \rho_{\text{elastic}} + \rho_{\text{inelastic}}$ ) [43]. During elastic

scattering, the resistivity gets suppressed while during inelastic scattering the resistivity gets enhanced with lowering the temperature and, hence, resistivity upturn is found at low temperature. The mechanism behind resistivity upturn can be understood by different processes, i.e. grain boundary localization (GB effect) [25], kondo effect [26], electrostatic blockade model [20], electron–electron scattering mechanism [44,45], etc. Since, present case of LPCMO manganite compound is of polycrystalline system and, hence, grain boundary effect can be eliminated in this investigation. Also, electrostatic blockade model can be employed for the nanostructured manganite systems thereby we have not concentrated on this model at present. Two remaining theoretical models were fitted to understand the resistivity upturn mechanism based on the scattering of electrons. Among them, first one is kondo effect and second is electron–electron scattering mechanism. Representation of kondo effect can be formulated as:  $\rho = [1/(\sigma_0 + B \ln T) + \rho_n T^n]$  [46–48] while electron–electron scattering mechanism can be expressed as:  $\rho = [1/(\sigma_0 + B T^{1/2})] + \rho_n T^n$  [49–52], where  $\sigma_0$  is the residual conductivity,  $B$  is related to the depth of the upturn and  $n$  is the power exponent. In both the formulae, the first term is related to elastic scattering and the second term is related to inelastic scattering between the electrons. Syskakis et al. [46] have observed the kondo like effect, i.e. logarithmic variation in resistivity, between 4 and 20K temperatures for Co impurity doped La<sub>0.75</sub>Sr<sub>0.20</sub>MnO<sub>3</sub> manganites. Wu et al. [47] have also observed a strong kondo effect for La<sub>0.7</sub>Ca<sub>0.3</sub>Mn<sub>1-x</sub>CrxO<sub>3</sub> manganites well below their freezing temperatures. Reshi et al. [48] have investigated ferromagnetic clusters of La<sub>0.7</sub>Sr<sub>0.3</sub>MnO<sub>3</sub> nanostructures and found dominant kondo effect at low temperatures well below 50K. Krichene et al. [49] have investigated the effect of Bi doping at Mn site in La–Ca based charge ordered manganites wherein  $T^{1/2}$  dependent resistivity (i.e. electron–electron scattering effect) has been discussed for low temperature region under different applied magnetic fields. Same research group has studied the La<sub>0.4</sub>Sm<sub>0.1</sub>Ca<sub>0.5</sub>MnO<sub>3</sub> charge ordered manganite and low temperature resistivity minimum anomaly has been observed and ascribed to the electron–electron scattering mechanism through the coulombic interactions [50]. Similar group has also understood the low temperature resistivity minimum behavior of phase separated charge ordered La<sub>0.4</sub>Dy<sub>0.1</sub>Ca<sub>0.5</sub>MnO<sub>3</sub> manganite in the context of electron–electron scattering [51].  $T^{1/2}$  dependent resistivity at low temperatures has been discussed in detail for La<sub>0.4</sub>Gd<sub>0.1</sub>Ca<sub>0.5</sub>MnO<sub>3</sub> manganite compound which justify an electron–electron scattering mechanism as a responsible process for resistivity minimum behavior [52]. In addition, generally, at low temperatures, it is believed that with decrease in temperature, the thermal energy gets suppressed thereby resistance of every metal gets suppressed upon reduction in the temperature. Even if, at the same low temperatures, due to the coulombic interactions between the charge carriers (i.e. electrons in metals as well as in mixed valent manganite systems), resistance values are controlled by the competition between (i) thermal energy induced reduction in resistance and (ii) coulombic interactions induced increase in resistance with decrease in temperature. When coulombic interaction effect becomes dominant, resistivity upturn comes into the picture which can be explained on the basis of electron–electron scattering mechanism. For kondo effect, one can consider the interaction between the free charge carries of metals (including mixed valent manganites) and existing magnetic impurities within the magnetic (metallic) lattice of these metals (mixed valent manganites). In this regard, it is expected that the movements of free charge carriers get affected by these magnetic impurities (which can be various defects including oxygen vacancies and grain boundaries within the lattice of mixed valent manganites) thereby resistivity gets increased with decrease in temperature at low temperature region. In actual sense, these free charge carriers (conduction electrons) are scattered by the magnetic impurities which can be explained on the basis of kondo effect at low temperatures. In short, electron–electron scattering process suggests that charge carriers are scattered by other charge carriers only within the lattice whereas kondo effect suggests that charge carriers are scattered by existing magnetic impurities within the lattice. By taking

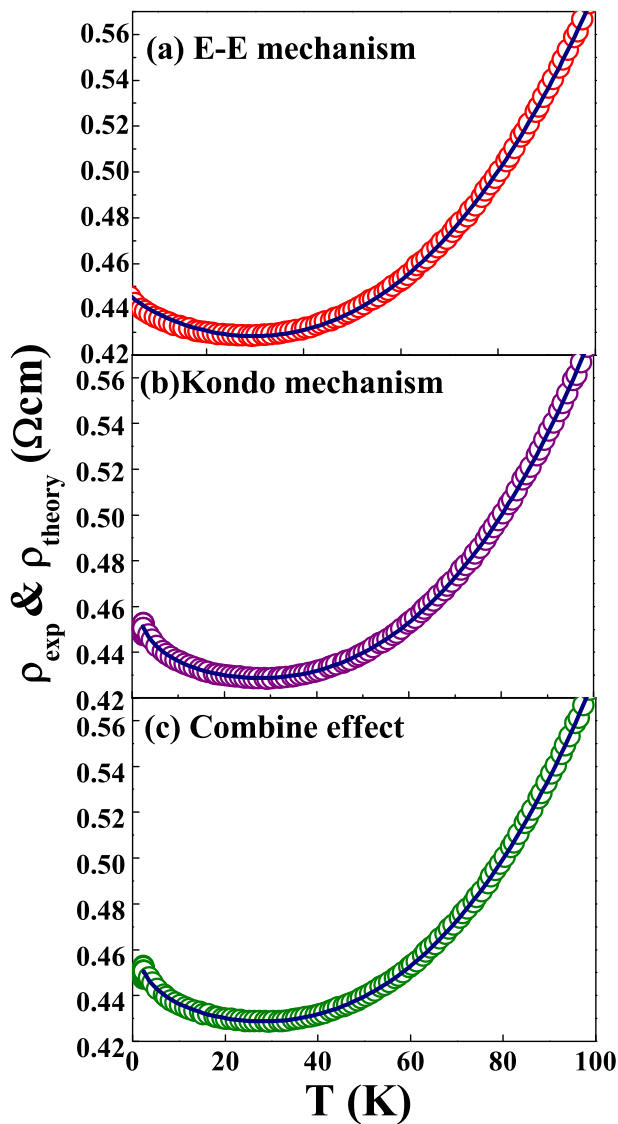


**Fig. 4.** Low temperature resistivity (temperature range: 5–100K) fits to (a) the electron–electron scattering mechanism:  $\rho = [1/(\sigma_0 + BT^{1/2})] + \rho_n T^n$ , (b) the kondo effect:  $\rho = [1/(\sigma_0 + B \ln T)] + \rho_n T^n$  and (c) the combine effect:  $\rho(T) = \rho_0 + \rho_e T^{1/2} - \rho_k \ln T^{1/2} + \rho_n T^n$  under zero field for LPCMO sample.

both these models into account, resistivity of the LPCMO sample was theoretically fitted for the temperature range of 5–100K, as shown in Fig. 4.

Fig. 4 shows the theoretical fits of (a) kondo effect and (b) electron–electron scattering effect for resistivity upturn (under zero field) for LPCMO manganite in the temperature range of 5–100K. At first glance, it can be seen that both the models fit well to the experimental data of  $\rho$ –T plot throughout the studied temperature range. Kondo effect can be expected in few manganite systems [46–48] and electron–electron scattering arises from enhanced columbic interactions present in the disordered metallic systems [49–52]. As these both cases are possible for currently studied system, it is useful to consider such model which includes both kondo effect and electron–electron scattering process, simultaneously. Few reports are available on the consideration of simultaneous effect (i.e. combined effect) of, both, electron–electron scattering mechanism and kondo effect to understand the low temperature resistivity minimum behavior for a single compound [53–56]. This unusual combined effect can be rarely found that explains resistivity upturn behavior in few manganites when the simultaneous effect of (i) charge carrier scattering through coulombic interactions and charge

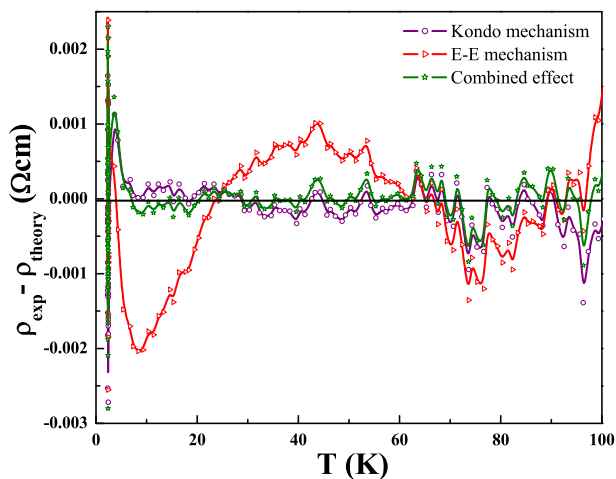


**Fig. 5.** The resistivity difference ( $\rho_{\text{exp}} - \rho_{\text{theory}}$ ) vs. T plot for resistivity minima models (kondo effect, electron–electron scattering mechanism and combined effect) under zero applied magnetic field for LPCMO manganite.

carrier scattering though magnetic impurity in magnetic metals (i.e. mixed valent manganites) overcome the thermal energy effect on charge conduction. These both effects can be combined [53–56] by the expression:  $\rho(T) = \rho_0 + \rho_e T^{1/2} - \rho_k \ln T^{1/2} + \rho_n T^n$ , where,  $\rho_0$  is residual resistivity,  $\rho_e$  and  $\rho_k$  are the contributions from electron–electron scattering and kondo mechanism, respectively and  $\rho_n$  is related to electron–phonon coupling. To understand the low temperature resistivity minimum behavior observed for magnetoresistive  $\text{La}_{0.7}\text{Ca}_{0.3}\text{MnO}_3$  manganite films, Kumar et al. [53] have employed a theoretical model based on the combination of, both, kondo effect and electron–electron scattering mechanism. Temperature and magnetic field dependent strong competition between the kondo effect and electron–electron scattering mechanism has been identified by employing the same combined model for solid state reaction prepared  $\text{La}_{2/3}\text{Sr}_{1/3}\text{MnO}_3$  manganite [54]. A series of samples of  $\text{La}_{0.67}\text{A}_{0.33}\text{MnO}_3$  ( $\text{A} = \text{Ca}, \text{Sr}, \text{Pb}$  and  $\text{Ba}$ ) manganites have been investigated for low temperature transport properties and found low temperature resistivity minima which has been attributed to the combined effect of kondo model, electron–electron scattering mechanism and electron–phonon interaction process [55]. Niu et al. [56] have also identified that resistivity minimum behavior of  $\text{La}_{0.7}\text{Sr}_{0.3}\text{MnO}_3$  ultra thin films can be better explained by a combined effect of kondo model and electron–electron scattering mechanism than separate model or mechanism. Fig. 4(c) shows the resistivity upturn fitted with combined effect under zero field. In the present case of LPCMO manganite, one can also consider the better suitability of kondo effect or its active governance over the low temperature resistivity minimum behavior of LPCMO manganite (in its combined model form) due to fact that: 10% (or even less) doping of smaller magnetic  $\text{Pr}^{3+}$  ions at larger  $\text{La}^{3+}$  ionic sites in LPCMO manganite creates large magnetic inhomogeneity within its lattice [30]. This inhomogeneity may serve more disorders in the lattice thereby various possible scattering centers for the charge carriers which are again magnetic in nature. This, and hence, supports the possibility or contribution from the kondo effect at low temperature resistivity minimum anomaly in the present LPCMO manganite. To verify the most suitable mechanism for charge conduction in low temperature region, temperature dependent the resistivity difference between experimental data and theoretical data ( $\rho_{\text{exp}} - \rho_{\text{theory}}$ ) vs T is plotted in Fig. 5. It shows that the combined effect is more appropriate mechanism to understand the resistivity upturn in LPCMO sample under study. Altintas et al. [22] have also identified similar combined effect for the understanding of low temperature resistivity upturn behavior of Eu based LRCMO (i.e.  $\text{La}_{0.6}\text{Eu}_{0.1}\text{Ca}_{0.3}\text{MnO}_3$ ) compound.

Fig. 6 shows the resistivity data in the temperature range of 5–100K under different applied magnetic fields fitted theoretically with

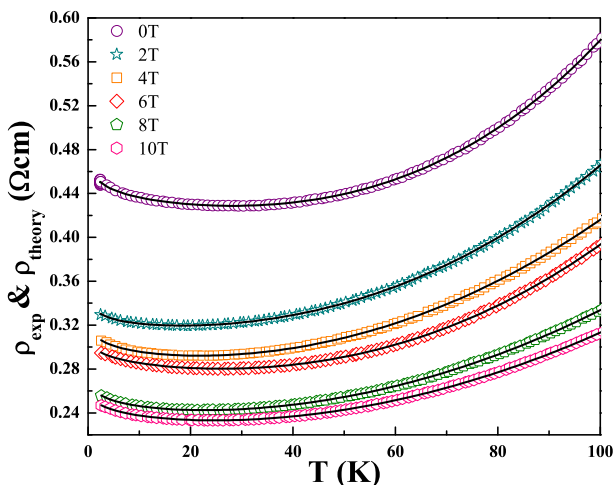


**Fig. 6.** Low temperature resistivity (temperature range: 0–100K) fits to the combine effect:  $\rho(T) = \rho_0 + \rho_e T^{1/2} - \rho_k \ln T^{1/2} + \rho_n T^n$ ) under different applied magnetic fields for LPCMO manganite.

combined effect of resistivity upturn for LPCMO sample. The values of all the fitting parameters are shown in Table 2. As shown in Table 2, all resistivities get reduced with increase in applied magnetic field which confirms the negative MR in the system within the temperature range of 5–100K. Exponent n also found to decrease with increase in applied magnetic field that suggests the reduction in the scattering of the charge carriers and suppression in the spin vibrations in the LPCMO lattice under study. Overall  $\chi^2$  values, i.e. goodness of the fits, are found to be much smaller (in the range of 1E-8) that supports the suitability of the model employed for the study of resistivity upturn behavior.

An attempt has also been made to understand the charge transport mechanisms responsible for the metallic region of LPCMO sample. To understand the metallic nature of the presently studied sample, few theoretical models have been reported. Here, two theoretical models, namely, (i) ZDE polynomial law and (ii) small polaron conduction mechanism have been employed [57–59]. The ZDE polynomial law can be formulated as:  $\rho = \rho_0 + \rho_e T^2 + \rho_n T^n$  [35,60–62], where  $\rho_0$  is the residual resistivity,  $\rho_e$  is the resistivity contribution from electron-electron, electron-phonon and electron-magnon scatterings,  $\rho_n$  is higher order resistivity term and n is power exponent coefficient. Rathod et al. [35] have understood the metallic regions of nonmagnetic Al doped  $\text{La}_{0.7}\text{Ca}_{0.3}\text{Mn}_{1-x}\text{Al}_x\text{O}_3$  manganites ( $x = 0.00, 0.02, 0.04, 0.06, 0.08$  and  $0.10$ ) on the basis of ZDE mechanism and found that there is no considerable effect of magnetic field on electron-magnon processes for  $x < 0.10$  whereas for  $x = 0.10$  sample, two magnon scattering processes (under zero and 5T magnetic field) get suppressed by magnetic field and governed by one magnon scattering processes under 8T magnetic field. Gadani et al. [60] have investigated the interfacial resistance behavior of  $\text{LaMnO}_{3-\delta}/\text{La}_{0.7}\text{Ca}_{0.3}\text{MnO}_3/\text{LaAlO}_3$  heterostructures grown using two different chemical methods and found a metallic nature of the interfaces between the two manganite layers for the temperature range 5 to 300K. ZDE mechanism has been employed for both the interfaces (one grown

using wet chemical method and other using dry chemical method) to understand their metallic nature between the temperatures 5 and 225K. They found one magnon scattering mechanism for wet chemical process grown interface whereas two magnon scattering mechanism is governing the metallic behavior of the interface grown using dry chemical method. Similar heterostructures have again been studied for their metallic nature under different applied electric field using the ZDE polynomial law and same group has identified that the electron-magnon scattering mechanisms are strongly influenced by growth process as well as applied electric field [61]. Similar observations have been reported for  $\text{ZnO}/\text{La}_{0.7}\text{Ca}_{0.3}\text{MnO}_3/\text{LaAlO}_3$  and  $\text{LaMnO}_{3-\delta}/\text{La}_{0.7}\text{Ca}_{0.3}\text{MnO}_3/\text{LaAlO}_3$  heterostructures grown using the wet chemical method and found that electric field is an important parameter that affects the electron-magnon scattering processes for the studied low power operated heterostructure based devices [62]. The small polaron conduction mechanism can be expressed as:  $\rho = \rho_0 + [\text{A}\omega_s / \{\sinh^2(\hbar\omega_s / 4\pi K_B T)\}] + BT^n$  [63,64], where,  $\omega_s$  is an average frequency of softest optical mode. Sagapariya et al. [63] have prepared the bilayered film of  $\text{ZnO}/\text{La}_{0.7}\text{Sr}_{0.3}\text{MnO}_3/\text{Al}_2\text{O}_3$  using chemical solution deposition method. They have studied its resistivity behavior and theoretically fitted its metallic nature using the small polaron conduction mechanism. They could identify that their observed metallic behavior is governed by ZDE mechanism in better way than small polaron conduction mechanism. Chen et al. [64] have observed that ferromagnetic metallic region based resistivity data can be theoretically fitted successfully using small polaron conduction mechanism. Fig. 7 shows the theoretical fittings of  $\rho$ -T plots in the temperature range of 70–220K for (a) small polaron conduction mechanism and (b) ZDE polynomial law. Fig. 7 shows that both the models fit very well to the experimental resistivity data in the employed temperature range. To confirm the most preferable mechanism for the charge conduction in metallic region, temperature dependent resistivity difference between experimental data and theoretical data ( $\rho_{exp} - \rho_{theory}$ ) is plotted, as shown in Fig. 7(c). It can be observed that the ZDE polynomial law is followed better by resistivity in metallic region of LPCMO sample under zero field. To evaluate the effect of magnetic field on the charge conduction in the metallic region of LPCMO sample, temperature dependent resistivity data (within the temperature range: 70–220K) were fitted using ZDE polynomial law, as shown in Fig. 8. For ZDE polynomial law, value of parameter n gives information about the charge conduction process in the respective material, i.e. value of n between 2.5 and 3 relates to the one magnon scattering and n = 4.5 and 7.5 relate to the two magnon scattering process while n may be ~ 5.5 and 6.5 for intermediate order of scatterings and spin fluctuations. Higher values of n, more than this, can be ascribed to higher order spin fluctuations in magnetic lattice of manganites. For presently studied sample, the variation in values of n for all applied magnetic fields are shown in Fig. 9. The plot shows that the power exponent n decreases with the increase in applied magnetic field which can be related to the field induced suppression of spin fluctuations. For LPCMO sample, value of n varies between 11.52 (0T) and 3.22 (10T) which gives explanation about reduced spin fluctuations and improved ZDE mechanism under higher applied magnetic fields. The theoretical fitting parameters of ZDE polynomial law in the metallic region for LPCMO sample are listed in Table 3. From Table 3, it can be understood that  $\rho_0$  which is the temperature independent resistivity term (due to the domain and grain boundary contributions) decreases with applied magnetic field. With increasing magnetic field, the size of the domain boundary diminishes and, hence, the value of  $\rho_0$  also decreases. It is found that the value of  $\rho_n$  (electron-magnon scattering term) decreases with increasing magnetic field indicating the suppression of magnetic fluctuations in accordance with the increase in applied magnetic field. Reported LRCMO compounds with R = Eu [22], Y [40], Ho [41] and Y [41] have been understood for their metallic regions by considering similar polynomial (like ZDE of present case) law with fixed value of n = 4.5 (in all these reports), i.e. two magnon scattering process, whereas in the present case it can be understood that the scattering process get modified upon change in applied magnetic field (Fig. 9 and Table 3).

**Table 2**

Values of parameters derived from the fittings of combine effect (electron-electron scattering mechanism and kondo effect) for LPCMO manganite.

H (T)	$\rho_0$ ( $\Omega$ cm)	$\rho_e$ ( $\Omega$ cm/ $K^{1/2}$ )	$\rho_k$ ( $\Omega$ cm/ K)	$\rho_n$ ( $\Omega$ cm/ $K^n$ )	n	$\chi^2$
0	0.45974	0.00304	0.00853	5.7439E-6	2.973	5.1187E-8
2	0.33569	0.00283	0.00774	4.6223E-6	2.550	4.8642E-8
4	0.31477	0.00168	0.00624	3.7760E-6	2.490	4.2410E-8
6	0.30325	0.00157	0.00588	1.9368E-6	2.294	4.1748E-8
8	0.26400	0.00122	0.00397	1.6280E-6	2.193	2.8844E-8
10	0.25558	0.00096	0.00396	1.0868E-6	2.133	1.1096E-8

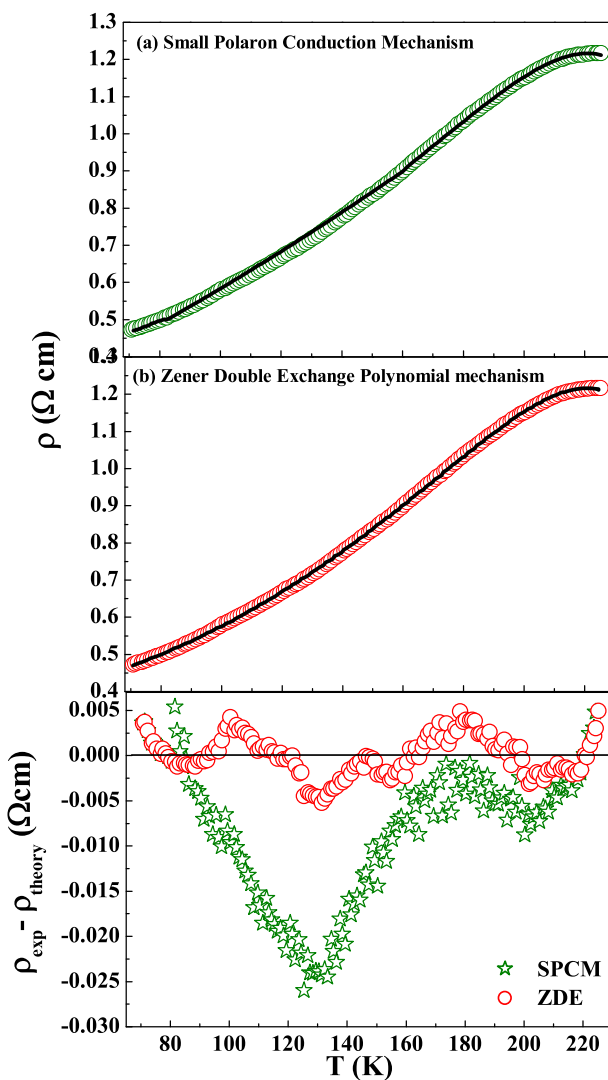


**Fig. 7.** Temperature dependent resistivity (temperature range: 70–220K) fits to (a) small polaron conduction mechanism:  $\rho = \rho_0 + [A\omega_0/\sinh^2(h\omega_0/4\pi K_B T)] + BT^n$  and (b) ZDE polynomial law:  $\rho = \rho_0 + \rho_2 T^2 + \rho_n T^n$ , under zero applied magnetic field for LPCMO sample and (c) resistivity difference ( $\rho_{\text{exp}} - \rho_{\text{theory}}$ ) vs. T plot for both above models under zero field for LPCMO sample.

The LPCMO sample exhibits insulating/semiconducting behavior above their respective  $T_p$  under all the studied magnetic fields. Several models have been employed to understand the charge transport mechanism above  $T_p$  till present day, i.e. small polaron conduction mechanism for semiconducting nature of manganites [65], nearest neighbor hopping mechanism [66], Schklovskii-Efross type variable range hopping (VRH) mechanism [67] and Mott type VRH model [68,69]. Among them, following three theoretical models have been fitted to experimental resistivity data under zero field, namely, (i) nearest neighbor hopping mechanism:  $\rho = \rho_0 \exp(E_a/KT)$  [70], (ii) small polaron conduction mechanism:  $\rho = AT \exp(E_a/KT)$  [71–73] and (iii) Mott type VRH mechanism:  $\rho = \rho_0 \exp(T_0/T)^{1/4}$  [74–76]. Drozd et al. [70] employed various models and mechanisms including thermally activated nearest neighbor hopping mechanism for understanding the resistivity behavior of semiconducting region of various rare earth (RE) elements doped  $\text{La}_{0.75-x}\text{RE}_x\text{Ca}_{0.25}\text{MnO}_3$  manganite systems. Ghani et al. [71], have investigated the charge conduction mechanism for semiconducting region based resistivity behavior of bismuth based  $\text{La}_{0.7-x}\text{Bi}_x\text{Ce}_{0.3}\text{MnO}_3$  ceramics on the basis of small polaron conduction mechanism and estimated an activation energy for all the manganite ceramics studied. Similar model has also been employed for semiconducting nature of

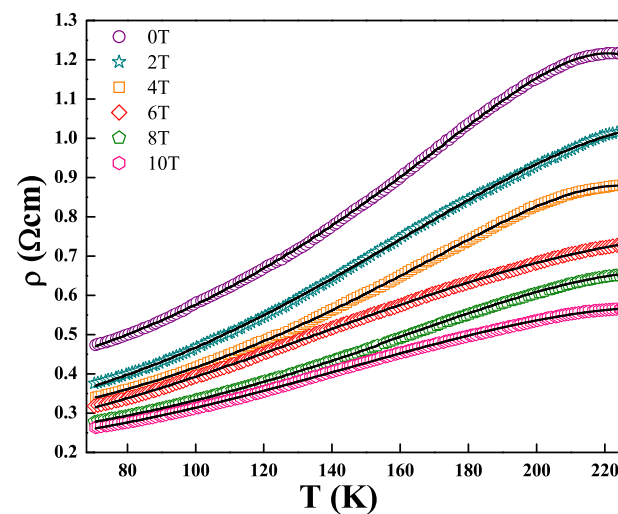


**Fig. 8.** Low temperature resistivity (temperature range: 70–220K) fitted using the ZDE polynomial law:  $\rho_0 + \rho_2 T^2 + \rho_n T^n$  under different applied magnetic fields for LPCMO sample.

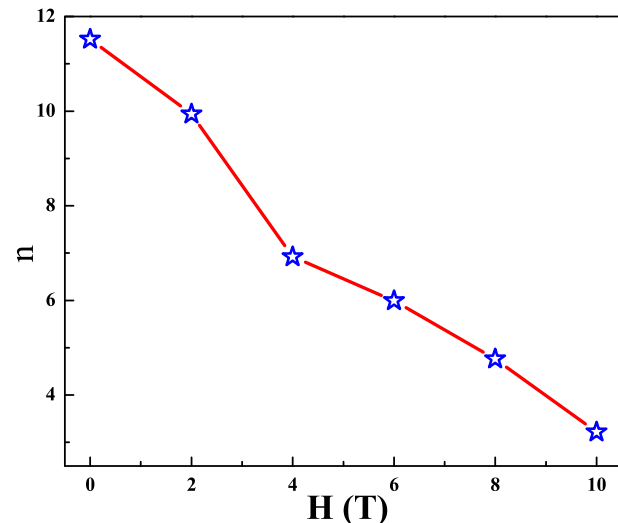


**Fig. 9.** Variation in the power exponent (n), obtained from resistivity fits using ZDE polynomial law with the applied magnetic field for LPCMO sample.

**Table 3**

Values of residual resistivity ( $\rho_0$ ),  $\rho_2$ , higher order resistivity ( $\rho_n$ ), power exponent (n), and goodness of fits ( $\chi^2$ ) obtained from Zener double exchange polynomial law fits to low temperature (70–220 K) resistivity behavior for LPCMO manganite.

H (T)	$\rho_0$ ( $\Omega \text{ cm}$ )	$\rho_2$ ( $\Omega \text{ cm}$ )	$\rho_n$ ( $\Omega \text{ cm}$ )	N	$\chi^2$
0	0.36484	0.00002	2.393E-7	11.52	8.4096E-6
2	0.27276	0.00002	2.218E-6	9.94	5.2008E-6
4	0.26337	0.00002	2.159E-6	6.92	3.4035E-7
6	0.22619	0.00002	1.998E-5	5.99	2.1495E-6
8	0.22405	0.00001	1.756E-4	4.76	1.9681E-8
10	0.22363	0.00001	1.410E-4	3.22	1.6884E-6

resistivity data for  $\text{La}_{1-x}\text{K}_x\text{MnO}_3$  manganite compounds [72] and  $\text{La}_{2/3}(\text{Ca}_{1-x}\text{Sr}_x)\text{MnO}_3$  manganite systems [73]. To estimate activation energy for  $\text{La}_{0.325}\text{Tb}_{0.125}\text{Ca}_{0.3}\text{Sr}_{0.25}\text{MnO}_3$  manganite compound under different applied magnetic fields, VRH model has been employed for semiconducting region of its resistivity behavior [74]. Similarly,  $\text{La}_{0.325}\text{Tb}_{0.125}\text{Ca}_{0.5}\text{MnO}_3$  manganite compound has also been studied for

its activation energy (for semiconducting behavior) under different applied magnetic fields using the same VRH model [75]. Recently, Krichene et al. [76] have also employed a similar VRH model for  $\text{Pr}_{0.45}\text{Bi}_{0.05}\text{Sr}_{0.5}\text{MnO}_3$  manganite compound for its resistivity data of semiconducting region. It can be observed that all the three models have been fitted well to resistivity data in semiconducting region (temperature range: 260–320K), as shown in Fig. 10. In these model fits, following aspects have been considered to decide the initial values of fits: (i) nearest neighbor hopping mechanism:  $\rho_0$  is a residual resistivity considered as the resistivity at lowest temperature studied (i.e. resistivity at 5K),  $K$  is a Boltzmann constant considered in its eV unit with  $K = 8.617 \times 10^{-5}$  eV/K and  $E_a$  is the estimated/derived activation energy from a fit, (ii) small polaron conduction mechanism:  $A$  is residual resistivity considered again as the resistivity at 5K,  $K$  is Boltzmann constant considered in eV unit and  $E_a$  is an activation energy derived using the fit and (iii) VRH mechanism:  $\rho_0$  is a residual resistivity considered as the resistivity at 5K and  $T_O$  has been derived from the nonlinear fit to the data. Using the value of  $T_O$ , activation energy has been calculated in its unit of eV (and discussed later in the present communication). To verify the most suitable charge conduction mechanism responsible for the semiconducting region of LPCMO sample under study, the difference between the experimental and theoretical resistivity data was calculated and plotted as a function of temperature under zero field as shown in Fig. 11. It can be seen from Fig. 11 that Mott type VRH model is suitable to understand the charge conduction mechanism in LPCMO sample. Fig. 12 shows the temperature dependent resistivity plots under different applied magnetic fields theoretically fitted using Mott type VRH model. The plots indicate a good agreement between the model fits and resistivity of semiconducting region suggesting that Mott type VRH model is obeyed by semiconducting resistivity behavior under all applied magnetic fields. In Mott type of VRH model,  $T_O$  indicates the charge carrier localization length. The values of activation energy at different magnetic fields have been calculated using the equation,  $T_O = E_a/K$ , where  $E_a$  is the activation energy and  $K$  is the Boltzmann constant ( $8.617 \times 10^{-5}$  eV/K). The calculated values of  $E_a$  are found to be reduced from 0.22eV to 0.16eV with applied magnetic field from 0 to 10T which can be correlated with the field induced suppression in charge carrier localization length that helps the charge carriers to hop across the Mn–O magnetic lattice thereby a reduction in activation energy is found (Fig. 13).

While comparing present results based on the insulating/semiconducting behavior of LPCMO compound with that obtained and reported for different rare earth based LRCMO compounds, it can be observed that presently studied LPCMO possesses activation energies between  $\sim 220$  meV under zero magnetic field and  $\sim 160$  meV under 10T applied magnetic field. These values are much higher than Eu based LRCMO compound [ $\sim 159$  meV (zero magnetic field) and  $\sim 144$  meV (7T applied magnetic field)] [22]. For estimating this energy, they have employed adiabatic small polaron hopping model. Y based compound also possesses much lower energy value ( $\sim 164$  meV) [40] than that of present case (i.e. 220 meV) under zero magnetic field wherein Y based compound has been understood for an activation energy on basis of small polaron conduction model. As reported by Choudhary et al. [42], similar to the present case, they have also employed VRH model to estimate activation energies for LRCMO compounds with  $R = \text{Nd}$  ( $5.058 \times 10^{-8}$  meV), Sm ( $8.376 \times 10^{-8}$  meV), Gd ( $9.332 \times 10^{-8}$  meV) and Dy ( $11.133 \times 10^{-8}$  meV). All these values are much lower than that for the present case of LPCMO manganite compound. The reported considerably lower values of an activation energy for different rare earth based LRCMO compounds [42] as compared to present case of LPCMO sample may be ascribed to the fact that other rare earth based LRCMO compounds (from pechini method) have nanosized particles, but the LPCMO in this work (from solid state reaction synthesis) has micron sized particles.

MR is one of the most important properties of the doped perovskite manganites. The LPCMO sample shows a decrease in resistivity with an increase in magnetic field indicating the presence of negative MR,  $\text{MR} (\%) = [(\rho_0 - \rho_H)/\rho_0] \times 100$ , where  $\rho_0$  and  $\rho_H$  are the resistivities

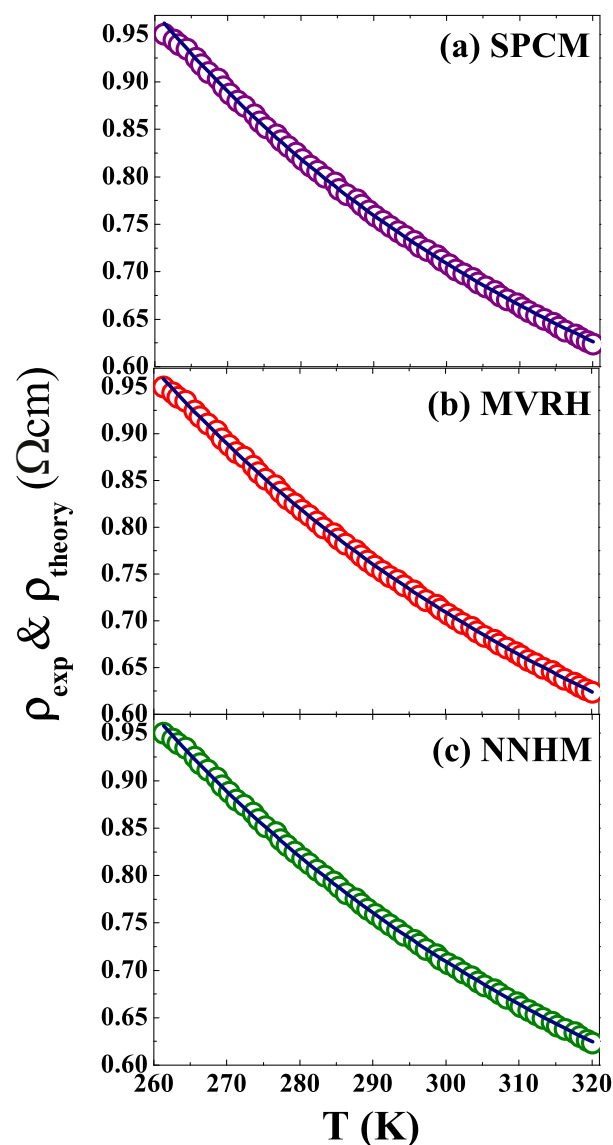


**Fig. 10.** Temperature dependent resistivity (temperature range: 260–320K) fits to (a) the small polaron conduction mechanism (SPCM):  $\rho = AT \exp(E_a/KT)$ , (b) Mott type VRH model (MVRH):  $\rho = \rho_0 \exp(T_o/T)^{1/4}$  and (c) nearest neighbor hopping mechanism (NNHM):  $\rho = \rho_0 \exp(E_a/KT)$  under zero applied magnetic field for LPCMO sample.

measured under  $H = 0$  and  $H$ , respectively. MR behavior of presently studied LPCMO sample was characterized at 5, 220, 265 and 300K as shown in Fig. 14. Negative MR increases with increase in applied magnetic field suggesting the improved spin orientation at the grain boundaries and, hence, improved charge conduction in the LPCMO lattice for all the temperatures studied.

As shown in Fig. 14, LPCMO sample shows a sharp rise in MR on application of 1T magnetic field, known as low field MR. This low field MR is the resultant effect of spin dependent scattering at 5K. As well as high field MR (extrinsic MR) at 5K can be ascribed to the reduced stiffness of the spins at the grain boundaries with the application of higher magnetic field ( $>1$ T). In this case, the conduction takes place through the connectivity between the grains. Furthermore, at the scenario of high field MR (intrinsic MR) at 220, 265, and 300K can be associated with the magnetic field dependent reduction in scattering of the charge carriers at grain boundaries and reduction in the magnetic lattice distortions.

To understand the variability in MR with magnetic field at different temperatures, theoretical fits of MR vs.  $H$  have been taken into

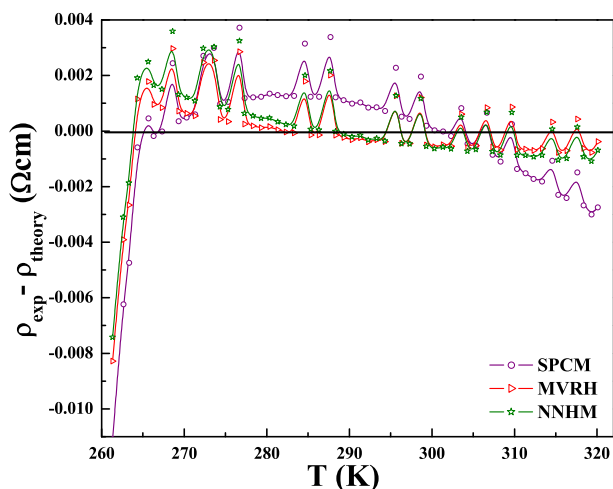


**Fig. 11.** Resistivity difference ( $\rho_{\text{exp}} - \rho_{\text{theory}}$ ) vs. T plot for semiconducting region for different employed theoretical models under zero field for LPCMO sample.

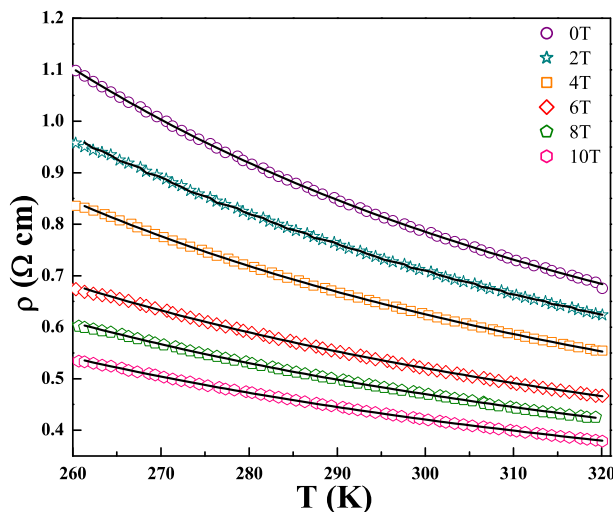


**Fig. 12.** Temperature dependent resistivity (temperature range: 260–320K) fitted using Mott type of VRH model:  $\rho = \rho_0 \exp(T_0/T)^{1/4}$  under different applied magnetic fields for LPCMO sample.

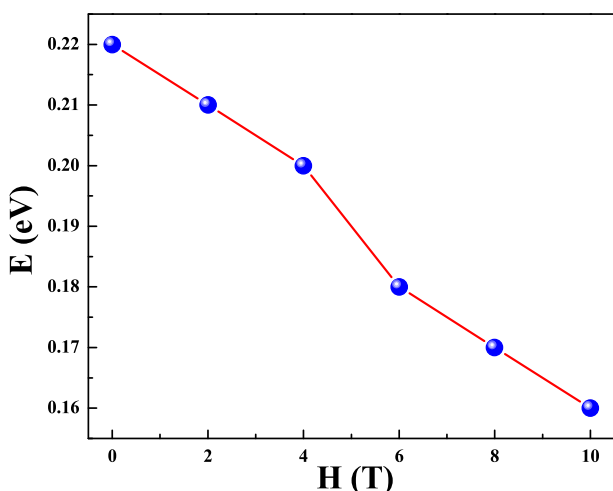


**Fig. 13.** Variation in the activation energy (E), obtained from resistivity fits using Mott type VRH model, with the applied magnetic field for LPCMO sample.

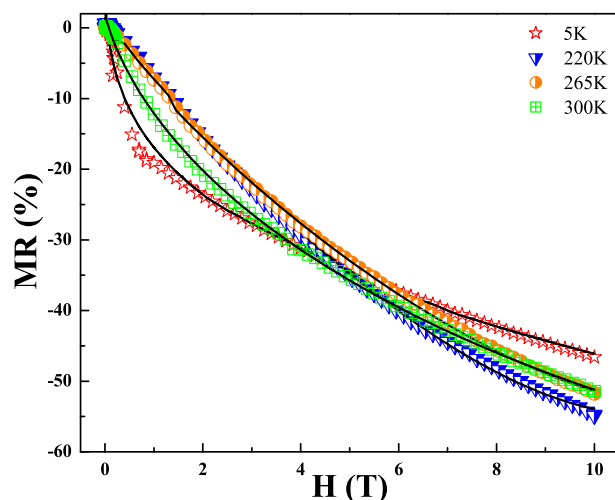


**Fig. 14.** Applied magnetic field dependent MR isotherms fits to (i)  $-\text{MR} (\%) = A \times \exp(B \times H) - C \times H^n$  at 5K and (ii)  $-\text{MR} (\%) = -A \times \exp(B \times H) + C \times H + D \times H^n$  at 220, 265 and 300K at different temperatures for LPCMO sample.

consideration. As both of grain and grain boundaries contribute for the mechanism of MR, following two theoretical fits were employed to differentiate their roles: (i)  $-\text{MR} (\%) = A \times \exp(B \times H) - C \times H^n$  [44], where  $A$  is the initial variation in resistivity under the small applied magnetic field, second term is related to grain boundary contribution, the third term deals with the small contribution of grains at low temperature and  $n$  represents the power exponent for MR vs.  $H$  isotherms and (ii)  $-\text{MR} (\%) = -A \times \exp(B \times H) + C \times H + D \times H^n$  [44], where the first term relates with the contribution from grain boundaries while last two terms are associated with the contribution from grain boundaries [44]. Vaghela et al. [44] have investigated the MR behavior (MR isotherms) at different temperatures for chemically grown pristine and swift heavy ions irradiated  $\text{La}_{0.7}\text{Pb}_{0.3}\text{MnO}_3$  manganite films having different thicknesses. They employed above mentioned MR models to identify the role and contribution of grains and grain boundaries in governing the MR behaviors of studied manganite films. At 5K, the equation (i) fits properly with the whole range of applied magnetic field while MR at 220, 250 and 300K follows the equation (ii). It suggests that at low temperatures, the grain boundary contribution becomes dominant and for higher temperatures, contribution from grains is dominant.

On the basis of comparison for the MR values of LPCMO compound and reported LRCMO compounds, reported Eu based LRCMO compound (i.e.  $\text{La}_{0.6}\text{Eu}_{0.1}\text{Ca}_{0.3}\text{MnO}_3$ ) exhibits maximum negative MR  $\sim 34\%$  under 4T at 5K applied magnetic field [22] which becomes  $\sim 31\%$  under the same 4T field at 5K in the case of presently studied LPCMO manganite compound. Also, under an application of 1T magnetic field, reported Eu based manganite compound exhibits  $\sim 25\%$  MR at 5K [22] which is found to be suppressed ( $\sim 19\%$  under 1T at 5K) for the present case of LPCMO manganite sample. Both these observations, overall, suggest that presently studied sample possesses comparatively improved charge transport and conduction across its lattice (as discussed for  $T_p$  value and peak resistivity) than reported Eu based LRCMO compound [22] thereby less effect of magnetic field on the charge conduction and, hence, lower MR can be expected for the presently studied LPCMO manganite as compared to  $\text{La}_{0.6}\text{Eu}_{0.1}\text{Ca}_{0.3}\text{MnO}_3$  manganite compound [22].

#### 4. Conclusion

In conclusion, LPCMO was synthesized using solid state reaction method. LPCMO sample is crystallized in orthorhombic structure without any impurity, as confirmed through Rietveld refinements. Low temperature resistivity study for resistivity upturn, metallic behavior and insulating/semiconducting behavior has been discussed in the context of

different charge conduction mechanisms. Low temperature resistivity upturn exhibited by the sample has been attributed to the combined electron-electron scattering and kondo effects. The metallic nature of LPCMO sample has been testified with ZDE polynomial law as well as small polaron hopping conduction mechanism. It is found that ZDE polynomial law is more appropriate to understand the conduction mechanism for metallic nature of LPCMO sample under different applied magnetic fields. For insulating (semiconducting) region, three models have been fitted among which Mott type of VRH model is fitted more suitably to resistivity experimental data. Values of the activation energy at different magnetic fields have been calculated and are found to decrease with applied magnetic field which may be attributed to decrease in charge carrier localization length. Magneto-transport studies suggest the presence of negative MR at different temperatures for LPCMO manganite. To understand the contributions from grain and grain boundaries, MR isotherms have been fitted to different formulae that represent the separate contributions of the same.

### Declaration of competing interest

The authors declare that they have no known competing financial interests or personal relationships that could have appeared to influence the work reported in this paper.

### CRediT authorship contribution statement

**Sapana Solanki:** Investigation, Writing - original draft. **Davit Dhruv:** Investigation. **Hetal Boricha:** Formal analysis. **Alpa Zankat:** Formal analysis. **K.N. Rathod:** Data curation. **Bhargav Rajyaguru:** Software. **R.K. Trivedi:** Funding acquisition. **A.D. Joshi:** Software. **S. Mukherjee:** Methodology. **P.S. Solanki:** Writing - review & editing. **N.A. Shah:** Supervision, Validation.

### Acknowledgement

Resistivity/magnetoresistance measurements were performed at UGC-DAE Consortium for Scientific Research, Mumbai. Author RKT is thankful to UGC, New Delhi for financial support in the form of Minor Research Project (file no. 3-10/13/MRP-SEM/Policy file/UGC (WRO)/759/2014).

### References

- [1] S.F. Dubinin, V.E. Arkhipov, S.G. Teploukhov, Ya.M. Mukovskii, Ferromagnetic superstructure of an  $\text{La}_{0.85}\text{Sr}_{0.15}\text{MnO}_3$  manganite single crystal, *Phys. Solid State* 45 (2003) 118–123.
- [2] X.J. Chen, H.U. Habermeier, H. Zhang, G. Gu, M. Varela, J. Santamaría, C.C. Almasan, Metal–insulator transition above room temperature in maximum colossal magnetoresistance manganite thin films, *Phys. Rev. B* 72 (2005) 1–7, 104403.
- [3] S.B. Kansara, Davit Dhruv, Bharat Kataria, C.M. Thaker, S. Rayaprol, C.L. Prajapat, M.R. Singh, P.S. Solanki, D.G. Kuberkar, N.A. Shah, Structural, transport and magnetic properties of monovalent doped  $\text{La}_{1-x}\text{Na}_x\text{MnO}_3$  manganites, *Ceram. Int.* 41 (2015) 7162–7173.
- [4] D.P. Kozlenko, B.N. Savenko, Interplay between static cooperative Jahn–Teller distortion and magnetic properties of optimally doped manganites, *J. Phys. Condens. Matter* 16 (2004) 9031–9036.
- [5] J.C. Loudon, N.D. Mathur, P.A. Midgley, Charge-ordered ferromagnetic phase in  $\text{La}(0.5)\text{Ca}(0.5)\text{MnO}_3$ , *Nature* 420 (2002) 797–800.
- [6] D.G. Kuberkar, R.R. Doshi, P.S. Solanki, Uma Khachar, Megha Vagadia, Ashish Ravalia, V. Ganesan, Grain morphology and size disorder effect on the transport and magnetotransport in sol-gel grown nanostructured manganites, *Appl. Surf. Sci.* 258 (2012) 9041–9046.
- [7] A.K. Pramanik, A. Banerjee, Phase separation and the effect of quenched disorder in  $\text{Pr}_{0.5}\text{Sr}_{0.5}\text{MnO}_3$ , *J. Phys. Condens. Matter* 20 (2008) 1–10, 275207.
- [8] J.P. Zhou, J.T. McDevitt, J.S. Zhou, H.Q. Yin, J.B. Goodenough, Y. Gim, Q.X. Jia, Effect of tolerance factor and local distortion on magnetic properties of the perovskite manganites, *Appl. Phys. Lett.* 75 (1999) 8.
- [9] A.P. Ramirez, Colossal magnetoresistance, *J. Phys. Condens. Matter* 9 (1997) 8171–8199.
- [10] K.Y. Pan, S.A. Halim, K.P. Lim, W.M.W.Y. Daud, S.K. Chen, M. Navasery, Microstructure, electrical and magnetic properties of polycrystalline  $\text{La}_{0.85}\text{K}_{0.15}\text{MnO}_3$  manganites prepared by different synthesis routes, *J. Mater. Sci. Mater. Electron.* 24 (2013) 1869–1874.
- [11] B.I. Belevtsev, V.B. Krasovitsky, V.V. Bobkov, D.G. Naugle, K.D.D. Rathnayaka, A. Parasiris, Influence of high-energy electron irradiation on the transport properties of  $\text{La}_{1-x}\text{Ca}_x\text{MnO}_3$ , *Eur. Phys. J. B* 15 (2000) 461–468.
- [12] D.P. Kozlenko, V.P. Glazkov, Z. Jirák, B.N. Savenko, High pressure effects on the crystal and magnetic structure of  $\text{Pr}_{1-x}\text{Sr}_x\text{MnO}_3$  manganites ( $x = 0.5\text{--}0.56$ ), *J. Phys. Condens. Matter* 16 (2004) 2381–2394.
- [13] Zalak Joshi, D.D. Pandya, Davit Dhruv, Keval Gadani, Hetal Boricha, Sanjay Kansara, J.H. Markna, P.S. Solanki, N.A. Shah, Investigations on structural disorder-induced modifications in the transport behaviour of rare earth manganites, *Bull. Mater. Sci.* 39 (2016) 1109–1117.
- [14] Keval Gadani, M.J. Keshvani, Davit Dhruv, Hetal Boricha, K.N. Rathod, Pooja Prajapati, A.D. Joshi, D.D. Pandya, N.A. Shah, P.S. Solanki, Low field magnetoelectric and magnetotransport properties of sol-gel grown nanostructured  $\text{LaMnO}_3$  manganites, *J. Alloys Compd.* 719 (2017) 47–57.
- [15] Zalak Joshi, Davit Dhruv, K.N. Rathod, Hetal Boricha, Keval Gadani, D.D. Pandya, A.D. Joshi, P.S. Solanki, N.A. Shah, Low field magnetoelectric studies on the sol-gel grown nanostructured  $\text{Y MnO}_3$  manganites, *Prog. Solid State Chem.* 49 (2018) 23–36.
- [16] S. Othmani, M. Bejara, Dhahria, E.K. Hilil, The effect of the annealing temperature on the structural and magnetic properties of the manganites compounds, *J. Alloys Compd.* 475 (2009) 46–50.
- [17] Hardik Gohil, Hetal Boricha, K.N. Rathod, Keval Gadani, Bhargav Rajyaguru, A.D. Joshi, D.D. Pandya, K. Asokan, N.A. Shah, P.S. Solanki, Studies on transport properties of manganite based nano-micro particle–matrix composites, *J. Alloys Compd.* 775 (2019) 1016–1027.
- [18] P.K. Siwach, Pankaj Srivastava, Jai Singh, H.K. Singh, O.N. Srivastava, Broad temperature range low field magnetoresistance in  $\text{La}_{0.7}\text{Ca}_{0.3}\text{MnO}_3$ :nano-ZnO composites, *J. Alloys Compd.* 481 (2009) 17–21.
- [19] M. Ziese, S.P. Sena, Anisotropic magnetoresistance of thin  $\text{La}_{0.7}\text{Ca}_{0.3}\text{MnO}_3$  films, *J. Phys. Condens. Matter* 10 (1998) 2727–2738.
- [20] S.B. Kansara, Davit Dhruv, Zalak Joshi, D.D. Pandya, S. Rayaprol, P.S. Solanki, D.G. Kuberkar, N.A. Shah, Structure and microstructure dependent transport and magnetic properties of sol-gel grown nanostructured  $\text{La}_{0.6}\text{Nd}_{0.1}\text{Sr}_{0.3}\text{MnO}_3$  manganites: role of oxygen, *Appl. Surf. Sci.* 356 (2015) 1272–1281.
- [21] A. Krichene, W. Boujelben, A. Cheikhrouhou, Structural, magnetic and magnetocaloric properties in  $\text{La}_{0.5-x}\text{Re}_x\text{Ca}_{0.5}\text{MnO}_3$  manganites ( $x = 0, 0.1$  and  $\text{Re} = \text{Gd}, \text{Eu}, \text{Dy}$ ), *J. Alloys Compd.* 550 (2013) 75–82.
- [22] S.P. Altintas, A. Amira, N. Mahamdioua, A. Varilci, C. Terzioglu, Effect of Eu doping on structural and magneto-electrical properties of  $\text{La}_{0.7}\text{Ca}_{0.3}\text{MnO}_3$  manganites, *J. Alloys Compd.* 509 (2011) 4510–4515.
- [23] V. Sen, N. Panwar, G.L. Bhalla, S.K. Agarwal, Structural, magnetotransport and morphological studies of Sb doped  $\text{La}_{2/3}\text{Ba}_{1/3}\text{MnO}_3$  ceramic perovskites, *J. Phys. Chem. Solid.* 68 (2007) 1685–1691.
- [24] R.I. Zainullina, N.G. Bebenin, L.V. Elokhina, V.V. Ustinov, Ya.M. Mukovskii, Elastic and magnetic properties of the  $\text{La}_{0.6}\text{Pr}_{0.1}\text{Ca}_{0.3}\text{MnO}_3$  single crystal, *Phys. Solid State* 53 (2011) 1328–1332.
- [25] E. Rozenberg, M. Auslender, I. Felner, G. Gorodetsky, Low-temperature resistivity minimum in ceramic manganites, *J. Appl. Phys.* 88 (2000) 2578–2582.
- [26] P.S. Solanki, R.R. Doshi, Ashish Ravalia, M.J. Keshvani, Swati Pandya, V. Ganesan, N.A. Shah, D.G. Kuberkar, Transport studies on  $\text{La}_{0.8-x}\text{Pr}_{0.2}\text{Sr}_x\text{MnO}_3$  manganite films, *Phys. B* 465 (2015) 71–80.
- [27] N. Sharma, A.K. Nigam, R. Pinto, N. Venkataramani, S. Prasad, G. Chandra, S.P. Pai, Giant magnetoresistance studies on  $\text{La}_{(0.8-x)}\text{R}_x\text{Sr}_2\text{MnO}_3$  thin films ( $\text{R} = \text{Pr}, \text{Nd}, \text{Gd}, \text{Ho}$ ), *J. Magn. Magn. Mater.* 166 (1997) 65–70.
- [28] C.M. Thaker, S. Rayaprol, Krushna Mavani, D.S. Rana, M.S. Sahasrabudhe, S.I. Patil, D.G. Kuberkar, Effect of Pr–Ca substitution, on the transport and magnetic behavior of  $\text{LaMnO}_3$  perovskite, *Pramana* 58 (2002) 1035–1039.
- [29] J. Yang, W.H. Song, Y.Q. Ma, R.L. Zhang, B.C. Zhao, Z.G. Sheng, G.H. Zheng, J.M. Dai, Y.P. Sun, Structural, magnetic and transport properties in the Pr-doped manganites  $\text{La}_{0.9-x}\text{Pr}_x\text{Te}_{0.1}\text{MnO}_3$  ( $0 \leq x \leq 0.9$ ), *Phys. Rev. B* 70 (2004) 1–8, 144421.
- [30] N.G. Bebenin, R.I. Zainullina, V.V. Ustinov, Ya.M. Mukovskii, Effect of inhomogeneity on magnetic, magnetocaloric, and magnetotransport properties of  $\text{La}_{0.6}\text{Pr}_{0.1}\text{Ca}_{0.3}\text{MnO}_3$  single crystal, *J. Magn. Magn. Mater.* 324 (2012) 1112–1116.
- [31] A.M. Balagurov, V. Yu Pomyakushin, V.L. Aksenen, N.M. Plakida, N.A. Babushkina, L.M. Belova, O. Yu Gorbenko, A.R. Kaul, P. Fischer, M. Gutmann, L. Keller, Behavior of the atomic and magnetic structure of  $\text{La}_{0.35}\text{Pr}_{0.35}\text{Ca}_{0.30}\text{MnO}_3$  at a metal–insulator phase transition, *JETP Lett.* 67 (1998) 705–711.
- [32] M.J. Keshvani, Savan Katba, Sadaf Jethva, Malay Udeshi, Bharat Kataria, Ashish Ravalia, D.G. Kuberkar, Studies on structural, morphological and electroresistance properties of sol-gel grown nanostructured  $\text{PrMnO}_3$ , *Mater. Sci. Eng. B* 218 (2017) 40–50.
- [33] F.M. Araujo-Moreira, P.N. Lisboa-Filho, S.M. Zanetti, E.R. Leite, W.A. Ortiz, Superconductivity in sintered-poly-crystalline  $\text{PrBa}_2\text{Cu}_3\text{O}_{7-\delta}$ , *Phys. B* 284–288 (2000) 1033–1034.
- [34] V.A. Meza, X. Graten, R.F. Jardim, L. Ben-Dor, Preparation and general physical properties of polycrystalline  $\text{PrBa}_2\text{Cu}_3\text{O}_{7-\delta}$  obtained from sol-gel precursors, *Braz. J. Phys.* 32 (2002) 731–738.
- [35] J.S. Rathod, M.J. Keshvani, P.S. Solanki, D.D. Pandya, Bharat Kataria, N.A. Shah, D.G. Kuberkar, Studies on charge transport in Al-doped  $\text{La}_{0.7}\text{Ca}_{0.3}\text{Mn}_{1-x}\text{Al}_x\text{MnO}_3$  manganites, *Phys. B* 478 (2015) 1–5.
- [36] N.G. Bebenin, Ferromagnetic manganites  $\text{La}_{1-x}\text{Ca}_x\text{MnO}_3$ , *Phys. Met. Metallogr.* 111 (2011) 242–259.

- [37] N.G. Bebenin, R.I. Zainullina, V.V. Ustinov, Y.M. Mukovskii, Magnetic properties of  $\text{La}_{0.7-x}\text{Pr}_x\text{Ca}_{0.3}\text{MnO}_3$  single crystals: when is banerjee criterion applicable? *J. Magn. Magn Mater.* 354 (2014) 76–80.
- [38] R.I. Zainullina, N.G. Bebenin, V.V. Ustinov, Y.M. Mukovskii, Elastic and magnetic properties of single-crystal  $\text{La}_{0.4}\text{Pr}_{0.3}\text{Ca}_{0.3}\text{MnO}_3$ , *Phys. Met. Metallogr.* 114 (2013) 390–394.
- [39] R. Cherif, E.K. Hlil, M. Ellouze, F. Elhalouani, S. Obbade, Magnetic and magnetocaloric properties of  $\text{La}_{0.6}\text{Pr}_{0.1}\text{Sr}_{0.3}\text{Mn}_{1-x}\text{Fe}_x\text{O}_3$  ( $0 \leq x \leq 0.3$ ) manganites, *J. Solid State Chem.* 215 (2014) 271–276.
- [40] Z. Mohamed, N. Ibrahim, M.A. Ghani, S.D. Safian, S.N. Mohamed, Structural and electrical transport properties of  $(\text{La}_{0.7-x}\text{Y}_x)\text{Ca}_{0.3}\text{MnO}_3$  manganites, *Respir. Physiol.* 12 (2019) 861–866.
- [41] V. Ravindranath, M.S. Ramachandra Rao, G. Rangarajan, Y. Lu, K. Klein, R. Klingeler, S. Uhlenbruck, B. Buchner, R. Gross, Magnetotransport studies and mechanism of Ho- and Y-doped  $\text{La}_{0.7}\text{Ca}_{0.3}\text{MnO}_3$ , *Phys. Rev. B* 63 (2001) 1–7, 18443.
- [42] N. Choudhary, M.K. Verma, N.D. Sharma, S. Sharma, D. Singh, Correlation between magnetic and transport properties of rare earth doped perovskite manganites  $\text{La}_{0.6}\text{R}_{0.1}\text{Ca}_{0.3}\text{MnO}_3$  ( $\text{R} = \text{La, Nd, Sm, Gd, and Dy}$ ) synthesized by pechini process, *Mater. Chem. Phys.* 242 (2020) 122482.
- [43] P.S. Solanki, R.R. Doshi, U.D. Khachar, R.J. Choudhary, D.G. Kuberkar, Thickness dependent transport and magnetotransport in CSD grown  $\text{La}_{0.7}\text{Pb}_{0.3}\text{MnO}_3$  manganite films, *Mater. Res. Bull.* 46 (2011) 1118–1123.
- [44] Eesh Vaghela, M.J. Keshvani, Keval Gadani, Zalak Joshi, Hetal Boricha, K. Asokan, D. Venkateshwarlu, V. Ganeshan, N.A. Shah, P.S. Solanki, Charge transport mechanisms in sol-gel grown  $\text{La}_{0.7}\text{Pb}_{0.3}\text{MnO}_3/\text{LaAlO}_3$  manganite films, *Phys. Chem. Chem. Phys.* 19 (2017) 5163–5176.
- [45] B. Arun, M.V. Suneesh, M. Vasundhara, Comparative study of magnetic ordering and electrical transport in bulk and nano-grained  $\text{Nd}_{0.67}\text{Sr}_{0.33}\text{MnO}_3$  manganites, *J. Magn. Magn. Mater.* 418 (2016) 265–272.
- [46] E. Syskakis, G. Choudalakis, C. Papastaikoudis, Crossover between kondo and electron-electron interaction effects in  $\text{La}_{0.75}\text{Sr}_{0.20}\text{MnO}_3$  manganite doped with Co impurity? *J. Phys. Condens. Matter* 15 (2003) 7735–7749.
- [47] B.M. Wu, B. Li, W.H. Zhen, N. Ausloos, Y.L. Du, J.F. Fagnard, P. Vandebemden, Spin-cluster effect and lattice-deformation-induced kondo effect, spin-glass freeing and strong phonon scattering in  $\text{La}_{0.7}\text{Ca}_{0.3}\text{Mn}_{1-x}\text{Cr}_x\text{O}_3$ , *J. Appl. Phys.* 97 (2005) 1–6, 103908.
- [48] H.A. Reshi, S. Pillai, R.S. Yadav, T.A. Para, U.P. Deshpande, T. Shripathi, V. Shelke, Kondo-like electronic transport and ferromagnetic cluster-glass behavior in  $\text{La}_{0.7}\text{Sr}_{0.3}\text{MnO}_3$  nanostructures, *RSC Adv.* 5 (2015) 85950–85956.
- [49] A. Krichene, P.S. Solanki, S. Rayaprol, V. Ganeshan, W. Boujelben, D.G. Kuberkar, B-site bismuth doping effect on structural, magnetic and magnetotransport properties of  $\text{La}_{0.5}\text{Ca}_{0.5}\text{Mn}_{1-x}\text{Bi}_x\text{O}_3$ , *Ceram. Int.* 41 (2015) 2637–3647.
- [50] A. Krichene, P.S. Solanki, D. Venkateshwarlu, S. Rayaprol, V. Ganeshan, W. Boujelben, D.G. Kuberkar, Magnetic and electrical studies on  $\text{La}_{0.4}\text{Sm}_{0.1}\text{Ca}_{0.5}\text{MnO}_3$  charge ordered manganite, *J. Magn. Magn. Mater.* 381 (2015) 470–477.
- [51] A. Krichene, W. Boujelben, S. Mukherjee, P.S. Solanki, N.A. Shah, Transport and magnetoresistance studies on polycrystalline  $\text{La}_{0.4}\text{Dy}_{0.1}\text{Ca}_{0.5}\text{MnO}_3$ : role of phase separation, *Acta Mater.* 131 (2017) 491–498.
- [52] A. Krichene, W. Boujelben, S. Mukherjee, P.S. Solanki, N.A. Shah, Effect of charge ordering and phase separation on the electrical and magnetoresistive properties of polycrystalline  $\text{La}_{0.4}\text{Eu}_{0.1}\text{Ca}_{0.5}\text{MnO}_3$ , *Phys. Chem. Chem. Phys.* 114 (2018) 21–27.
- [53] D. Kumar, J. Sankar, J. Narayan, R.K. Singh, A.K. Majumdar, Low-temperature resistivity minima in colossal magnetoresistive  $\text{La}_{0.7}\text{Ca}_{0.3}\text{MnO}_3$  thin films, *Phys. Rev. B* 65 (2002) 1–6, 094407.
- [54] Z. Chen, Y. Xu, Y. Su, S. Cao, J. Zhang, Resistivity minimum behavior and weak magnetic disorder characteristics in  $\text{La}_{2/3}\text{Ca}_{1/3}\text{MnO}_3$  manganites, *J. Supercond. Nov. Magnetism* 22 (2009) 465–469.
- [55] G. Lalitha, P.V. Reddy, Low-temperature resistivity anomalies and magnetic field-induced transitions in neodymium-based manganites, *Phys. Scripta* 82 (2010) 1–10, 045704.
- [56] W. Niu, M. Gao, X. Wang, F. Song, J. Du, X. Wang, Y. Xu, R. Zhang, Evidence of weak localization in quantum interference effects observed in epitaxial  $\text{La}_{0.7}\text{Sr}_{0.3}\text{MnO}_3$  ultrathin films, *Sci. Rep.* 6 (2016) 1–7, 26081.
- [57] Khushal Sagapariya, Keval Gadani, K.N. Rathod, Zalak Joshi, Hetal Boricha, Davit Dhruv, M.J. Keshvani, Bhargav Rajayaguru, S.B. Kansara, A.D. Joshi, K. Asokan, P.S. Solanki, N.A. Shah, Charge transport in chemically grown manganite based heterostructures, *Mater. Chem. Phys.* 224 (2019) 229–237.
- [58] G.M. Zhao, V. Smolyaninova, W. Prellier, H. Keller, Electrical transport in the ferromagnetic state of manganites: small-polaron metallic conduction at low temperatures, *Phys. Rev. Lett.* 84 (2000) 6086–6089.
- [59] D.S. Rana, C.M. Thaker, K.R. Mavani, D.G. Kuberkar, D.C. Kundaliya, S.K. Malik, Magnetic and transport properties of  $(\text{La}_{0.7-2x}\text{Eu}_x)(\text{Ca}_{0.3}\text{Sr}_x)\text{MnO}_3$ : effect of simultaneous size disorder and carrier density, *J. Appl. Phys.* 95 (2004) 4934–4939.
- [60] Keval Gadani, Davit Dhruv, Zalak Joshi, Hetal Boricha, K.N. Rathod, M.J. Keshvani, N.A. Shah, P.S. Solanki, Transport properties and electroresistance of a manganite based heterostructure: role of the manganite–manganite interface, *Phys. Chem. Chem. Phys.* 18 (2016) 17740–17749.
- [61] Keval Gadani, M.J. Keshvani, Bhargav Rajayaguru, Davit Dhruv, B.R. Kataria, A.D. Joshi, K. Asokan, N.A. Shah, P.S. Solanki, Current-voltage characteristics and electroresistance in  $\text{LaMnO}_{3-\delta}/\text{La}_{0.7}\text{Ca}_{0.3}\text{MnO}_3/\text{LaAlO}_3$  thin film composite, *Phys. Chem. Chem. Phys.* 19 (2017) 29294–29304.
- [62] Keval Gadani, Khushal Sagapariya, K.N. Rathod, Hetal Boricha, Bhargav Rajayaguru, V.G. Shrimali, A.D. Joshi, K. Asokan, N.A. Shah, P.S. Solanki, Charge transport studies on chemically grown manganite based heterostructures, *Curr. Appl. Phys.* 19 (2019) 563–569.
- [63] Khushal Sagapariya, D. Venkateshwarlu, Bhargav Rajayaguru, Keval Gadani, V.G. Shrimali, A.D. Pandya, E.P. Amaladass, N.A. Shah, P.S. Solanki, Transport properties and electroresistance of manganite based heterostructure, *Ceram. Int.* 45 (2019) 19456–19466.
- [64] X.J. Chen, H.U. Habermeier, C.L. Zhang, H. Zhang, C.C. Almasan, Spin wave scattering at low temperatures in manganite films, *Phys. Rev. B* 67 (2003) 1–4, 134405.
- [65] M. Ziese, C. Srinitiwawong, Polaronic effects on the resistivity of manganite thin films, *Phys. Rev. B* 58 (1998) 11519–11525.
- [66] G. Synder, R. Hiskes, S. Dicarolis, M. Beasley, T. Geballe, Intrinsic electrical transport and magnetic properties of  $\text{La}_{0.67}\text{Ca}_{0.33}\text{MnO}_3$  and  $\text{La}_{0.67}\text{Sr}_{0.33}\text{MnO}_3$  MOCV thin films and bulk material, *Phys. Rev. B* 53 (1996) 14434–14444.
- [67] A.L. Efros, B.L. Shklovskii, Coulomb gap and low temperature conductivity of disordered systems, *J. Phys. C Solid State Phys.* 8 (1975) L49–L51.
- [68] J.M.D. Coey, M. Viret, L. Ranno, K. Ounadjela, Electron localization in mixed-valence manganites, *Phys. Rev. Lett.* 75 (1995) 3910–3913.
- [69] M. Viret, L. Ranno, J.M.D. Coey, Colossal magnetoresistance of the variable range hopping regime in the manganites, *J. Appl. Phys.* 81 (1997) 4964–4966.
- [70] V. Drozd, M. Pekala, J. Kovac, I. Skorvanek, M. Szymanski, S. Nedilko, Structure and transport properties of  $\text{La}_{0.75-x}\text{RE}_x\text{Ca}_{0.25}\text{MnO}_3$  ( $\text{RE} = \text{Gd, Dy, Ho}; 0 \leq x \leq 0.75$ ) manganites, *Acta Phys. Pol.*, A 106 (2004) 751–758.
- [71] M.A. Ghani, S.N. Supardan, A.K. Yahya, Effect of Bi substitution on transport and magnetoresistance properties of electron-doped  $\text{La}_{0.7-x}\text{Bi}_x\text{Ce}_{0.3}\text{MnO}_3$  ceramics, *J. Supercond. Nov. Magnetism* 28 (2015) 1835–1841.
- [72] S. Das, T.K. Dey, Role of spin polarized tunneling in magnetoresistance and low temperature minimum of polycrystalline  $\text{La}_{1-x}\text{K}_x\text{MnO}_3$  ( $x = 0.05, 0.1, 0.15$ ) prepared by pyrolytic method, *Bull. Mater. Sci.* 29 (2006) 633–636.
- [73] F. Rivadulla, M. Otero-Leal, A. Espinosa, A. de Andres, C. Ramos, J. Rivas, J.B. Goodenough, Suppression of ferromagnetic double exchange by vibronic phase segregation, *Phys. Rev. Lett.* 96 (2006) 1–4, 016402.
- [74] R.R. Doshi, P.S. Solanki, P.S.R. Krishna, A. Das, D.G. Kuberkar, Magnetic phase coexistence in  $\text{Tb}^{+3}$  – and  $\text{Sr}^{+2}$  –doped  $\text{La}_{0.7}\text{Ca}_{0.3}\text{MnO}_3$  manganite: a temperature-dependent neutron diffraction study, *J. Magn. Magn. Mater.* 321 (2009) 3285–3289.
- [75] R.R. Doshi, P.S. Solanki, Uma Khachar, D.G. Kuberkar, P.S.R. Krishna, A. Banerjee, P. Chaddah, First order paramagnetic–ferromagnetic phase transition in  $\text{Tb}^{+3}$  doped  $\text{La}_{0.5}\text{Ca}_{0.5}\text{MnO}_3$  manganite, *Phys. B* 406 (2011) 4031–4034.
- [76] A. Krichene, W. Boujelben, S. Mukherjee, N.A. Shah, P.S. Solanki, Magnetic phase separation in polycrystalline  $\text{Pr}_{0.5-x}\text{Bi}_x\text{Sr}_0.5\text{MnO}_3$  ( $x \leq 0.15$ ), *Ceram. Int.* 45 (2019) 3849–3856.